Materials Advances

ROYAL SOCIETY OF CHEMISTRY

PAPER

View Article Online
View Journal | View Issue

Cite this: *Mater. Adv.*, 2023, 4, 5740

Towards N-rich solid polymer electrolytes for Li-ion batteries?†

L. Artigues,[ad] M. Deschamps,[bc] F. Salles,[a] V. Chaudoy,[d] V. Lapinte[a] and L. Monconduit*[ac]

Received 14th September 2023,
Accepted 15th October 2023

DOI: 10.1039/d3ma00494e

rsc.li/materials-advances

Solid polymer electrolytes (SPEs) are faced with many specifications to replace today's liquid organic electrolyte in Li-ion batteries. In this paper, a branched polyethyleneimine (BPEI) is proposed as a new SPE. Infrared and ^{13}C NMR spectroscopy and DFT modelling were combined to clarify the ionic conduction mechanisms and performance of this new kind of polymer electrolyte. To improve its mechanical properties, the BPEI was semi-interpenetrated in a PEO-based network. Afterwards to provide mechanical integrity and efficient ionic transport, inorganic fillers of different natures were added into the membranes: Al_2O_3, SiO_2, ZrO_2 and LAGP. For instance, the addition of 10 wt% SiO_2 resulted in an enhancement in ionic conductivity, reaching 2.2×10^{-4} S cm^{-1} at 80 °C. Furthermore, in a symmetric cell, improved cycling facing lithium metal, with a stable response over hundreds of hours without polarization, regardless of filler nature was observed.

Introduction

The ever-growing demand for efficient energy storage systems is leading to new emerging electrochemical systems called post-Li-ion technologies. One of the solutions considered is to use a lithium metal (Li^0) negative electrode which would potentially increase the energy density of a battery thanks to its 10 times superior theoretical capacity to the graphite used today as the negative electrode in conventional Li-ion systems. A drawback of this emerging Li metal battery (LMB) technology when used with a classic liquid electrolyte (a lithium salt dissolved in carbonate solvent) is the growth of metallic lithium deposits, broadly referred to as ''dendrites'', resulting in battery failure. This dendritic growth problem remains the primary bottleneck to implementing high-energy and fast-charging batteries, able to reduce the charging time from the present couple of hours to a few minutes.[1] A potential solution is to use a solid polymer electrolyte (SPE) that would act as a mechanical barrier, inhibiting the growth of metallic needles. Since Wright proved, in 1970,[2] that a solid-state matrix could act as a solvent, dissociating salts and transporting charged species, numerous polymers have been studied, including polyethers (poly(ethylene oxide) (PEO)[3]), polycarbonates (poly(trimethylene carbonate) (PTMC)[4] or polyethylene carbonate (PEC)[5]) or fluoropolymers like poly(vinylidene fluoride) (PVdF).[6] Among them, the class of nitrogen-rich polymers (NRPs) has little been studied, although they possess interesting properties for SPE application: in particular, the N-rich polymer analogous to PEO, where a secondary amine substitutes the oxygen atom, resulting in a polymer called poly(ethylenimine) (PEI).[7] PEI was chosen due to its closely spaced polar groups, good solvating ability for metal salts, high chemical versatility (the polymer backbone can be chemically modified), and low cohesive energy density. The higher donor number of –N– (*i.e.*, 60) than –O– (*i.e.*, 22) makes it a better candidate for dissolving lithium salts.[8,9] Branched PEI (BPEI) consists of a highly ramified structure where 3 amine types can be found: tertiary (N), secondary (NH) and primary (NH_2). It presents very poor mechanical properties at room temperature (RT), looking like viscous honey, and possesses a low glass transition temperature T_g, allowing easy ion transport through the matrix but providing no physical barrier to dendritic growth.

To overcome the concern over mechanical strength, one strategy consists of the formation of crosslinked networks within the electrolyte. Mechanical and thermal properties, and dimensional stability can be effectively improved by introducing a crosslinked structure into the polymeric host material. A variant is to use semi-interpenetrated networks (s-IPNs), where an inert and free polymer is entangled in the crosslinked structure.[10,11] The main advantage of this system lies in the possible synergy combining the physical, chemical, thermal, mechanical and electrical properties of the different macromers, by appropriately selecting these components and

[a] *ICGM, University of Montpellier, CNRS, ENSCM, Montpellier, France. E-mail: Laure.monconduit@umontpellier.fr*
[b] *CEMHTI, CNRS UPR 3079, Université d'Orléans, F45071 Orléans, France*
[c] *Réseau sur le Stockage Electrochimique de l'Energie (RS2E), CNRS FR3459, Amiens, France*
[d] *Technocentre Renault, 1 avenue du Golf, 78084 Guyancourt, France*

† Electronic supplementary information (ESI) available. See DOI: https://doi.org/10.1039/d3ma00494e

adjusting their relative proportions. A compromise between physical integrity and segmental movement of the chains is easily achieved.

As has frequently been reported in the literature, PEO-based SPEs reveal a failure when cycled with lithium metal and a positive electrode, using $LiFePO_4$ (LFP) as the active material, for instance. This failure behaviour can be monitored by the arbitrary appearance of 'voltage noise' during charge and discharge and can be attributed to Li-dendrite-induced cell micro short-circuits. By incorporating a PEO-based s-IPN thanks to thermal polymerization, this behaviour disappears, and an adequate charge/discharge cycling performance was even achieved at 40 °C by Homann *et al.*[12] The resulting SPE from this study shows an ionic conductivity of 3.7×10^{-6} S cm^{-1} at 40 °C and an electrochemical stability window (ESW) of up to 4.6 V *vs.* Li^+/Li.

Forming an s-IPN is also possible through photo-crosslinking. The properties of the designed membrane electrolytes (such as T_g, ionic conductivity or mechanical strength) can be adjusted by controlling the crosslinking density. The formed SPE containing 20 wt% of crosslinker reaches an ionic conductivity of 1.5×10^{-5} S cm^{-1} at RT and stability up to 4.2 V *vs.* Li^+/Li.[13]

Another potential solution to improve the properties of SPEs is the preparation of a composite or hybrid polymer electrolyte (CSPE or HSPE, respectively), consisting of the addition of inorganic fillers into the polymeric matrix. In this composite, each component retains its own properties, and new ones can be obtained by the interaction between each component in association. The addition of a filler to a PEO-based polymer electrolyte, for example, can improve the ionic conductivity and interfacial properties in contact with the electrode.[14] This is due to the fact that the amorphous phase of PEO is increased, and the recrystallization of PEO is hindered. In the 1980s, many researchers began to study hybrid polymer electrolytes. In all cases, the size and characteristics of the fillers are the key factors to improving the electrochemical properties of polymer electrolytes. In 1982, Weston and Steele[15] reported for the first-time hybrid electrolytes based on PEO. The mechanical properties and ionic conductivity of $(PEO)_8$–$LiClO_4$ were significantly improved by doping with an inert filler, alumina (Al_2O_3). Since this first study of an HSPE, many other metal oxides have been added to polymer electrolytes to improve their properties. Commonly used metal oxide fillers are Al_2O_3,[16–21] silica (SiO_2),[14,22–25] titanium dioxide (TiO_2),[26,27] zirconium dioxide (ZrO_2),[21,28–31] and other metal oxides.[32–34]

Herein, a full description of a polyethyleneimine-based SPE is proposed with improved mechanical properties by both the formation of a semi-interpenetrated network BPEI-based SPE and the addition of fillers. Specific attention has also been paid to following the Li transport mechanism in the BPEI, through a combination of IR, NMR and DFT analyses.

Experimental section

SPE membrane preparation

Branched poly(ethyleneimine) (BPEI, M_w = 25 000 g mol^{-1}), poly(ethylene glycol)dimethacrylate (PEGDMA, average M_w = 750 g mol^{-1}), LiTFSI (purity >99%) and absolute ethanol (≥99.8%) were purchased from Sigma-Aldrich and used as received. Azobisisobutyronitrile (AIBN) was used as a thermal radical initiator. AIBN was purified by recrystallization with methanol before use to remove products of decomposition limiting polymerization.

Concerning ceramic fillers, aluminium oxide nanopowder (Al_2O_3), 13 nm primary particle size (TEM), 99.8% trace metal basis and silica, fumed power (SiO_2), 7 nm, were purchased from Sigma-Aldrich. Zirconium (IV) oxide nanopowder (ZrO_2), 15 to 25 nm APS powder, 99% (metals basis excluding Hf), surface area 20–30 m^2 g^{-1} was purchased from Alfa Aesar. Finally, lithium aluminium germanium phosphate ($Li_{1.5}Al_{0.5}Ge_{1.5}(PO_4)_3$, LAGP), 300–500 nm, purity: 99.99% was purchased from MSE Supplies. All nanopowders were used as received.

The solid polymer electrolytes were prepared by the standard solution casting technique. Initially, BPEI were added to a suitable solvent:ethanol. The solutions were stirred at room temperature until a homogenous solution was obtained. The lithium salt, LiTFSI, was added to the polymer solution, respecting the stoichiometric ratio (N : Li = 50, calculating by dividing the number of moles of polymer repeat units to the number of moles of LiTFSI), followed by stirring until a transparent solution was achieved. Finally, the polymer salt solution was cast in a Teflon mold. Two drying steps were required to ensure total evaporation of solvents: at 70 °C, for 15 h in a ventilated oven and for 15 h in vacuum. The resulting SPEs were directly placed in a glove box for further analysis.

^{1}H and ^{13}C NMR spectra were recorded using a Bruker Advance DRX 400 (400 MHz). The external reference was tetramethylsilane (TMS) with chemical shifts given in ppm. Samples were diluted in 0.5 mL of deuterated solvents, deuterium oxide (D_2O) or chloroform-*d* ($CDCl_3$), depending on their solubility. In the ^{1}H NMR spectra of BPEI, all CH_2 signals resonate between δ = 2.5 and 2.7 ppm. Therefore, methylene groups with different amine substituents cannot be sufficiently separated for quantitative analysis. For this reason, a study concentrating on ^{13}C NMR was preferred where all structural atoms show well-separated signals in the typical area between 37 and 56 ppm. Additional signals from residual monomer traces (δ = 17.6 ppm in ^{13}C) could not be detected in the spectra recorded. This analysis permits the structure of BPEI polymer to be described and distinguishes the three types of amine: tertiary (N), secondary (NH) and primary (NH_2). After the assignment of all peaks in the spectra followed by the integration of each peak, the composition of BPEI is calculated as the percentage of the three types of amine groups in the structure. We used the values from the table in Fig. 1 to calculate the percentage of primary amines. The sum of the integration of signals 6 and 7 divided by the total contribution results in $(1.3810 + 1.2166) \times 100/13.0907 = 19.84\%$.

Differential scanning calorimetry (DSC) characterizations were performed to investigate the glass transition temperature of each pure sample or sample doped with LiTFSI. Analyses were carried out using a NETZSCH DSC200F3 calorimeter. The calibration was performed using adamantane, biphenyl, indium,

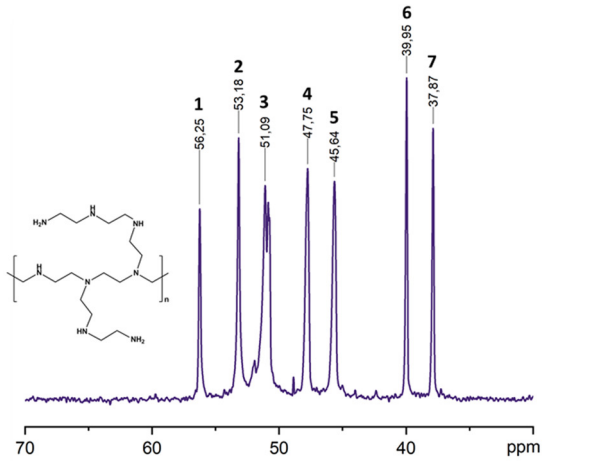

Signal number	Chemical shift (ppm)	Structural unit	Integration
1	56,25	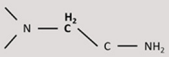	1
2	53,18	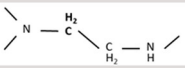	1,7969
3	51,09	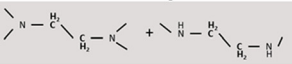	3,8005
4	47,75	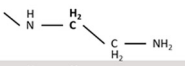	1,9123
5	45,64	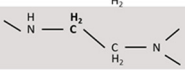	1,9834
6	39,95	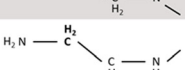	1,3810
7	37,87	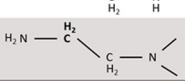	1,2166

Fig. 1 ^{13}C NMR spectrum of BPEI and the corresponding signal assignments.

tin, bismuth and zinc standards. Nitrogen was used as a purging gas. Samples were prepared in a glove box to avoid any contact with air or water contamination. Approximately 10 mg of the samples were placed in perforated aluminium pans and the thermal properties were recorded between −100 °C and 80 °C at 10 °C min^{-1}. The reported values were measured during the second heating ramp.

The thermal stability was tested by thermogravimetric analysis (TGA) on a TA TGA G50 instrument using a 40 mL min^{-1} flux of nitrogen as a purging gas. Samples were prepared in a glove box to avoid any contact with air or water contamination. Approximately 10 mg of samples were used for each analysis. Ramps from room temperature to 500 °C were applied at a rate of 20 °C min^{-1}.

The identification of interactions between polymer and salt was monitored by Fourier transform infrared (FTIR) spectroscopy regarding the shift in characteristic bands of typical groups. The analysis was realized on a PerkinElmer Spectrum 100 equipped with a ZnSe crystal using the ATR technique. Spectra were recorded in transmittance mode over the wavenumber region 4000–650 cm^{-1}.

DFT calculations were also carried out in order to determine the plausible geometry of the molecular system containing Li^+ in interaction with the polymer matrix. Furthermore, the interaction energy between polymer and Li^+ can be estimated from the difference between the energies of the global system {polymer-Li^+} and of the separate elements. Once the geometry optimization has been done, study of the phonons (corresponding to the bond vibrations) allows us to predict the infrared spectra and to compare them with the experimental data. The calculations were performed using DMol^3 from Materials Studio. Molecular models for BPEI polymers were built using 1 or 2 monomers in the presence or absence of Li^+. Additional configurations were calculated for LiTFSI (corresponding to Li^+ in interaction with $TFSI^-$), 2 LiTFSI in interaction and 2 BPEI in interaction. The parameters used for the geometric optimization considered the PBE GGA density functional, the double numerical basis set containing polarization functions on H atoms (DNP), and core treatment with all electrons taken into account. Formal spin was initially used for each atom while the spin was unrestricted during the calculations. The convergence was reached with the following criteria: energy variations lower than 10^{-5} Ha, maximal force variations lower than 0.002 Ha $Å^{-1}$, and maximum displacement variations lower than 0.005 Å.

Electrochemical impedance spectroscopy (EIS) measurements were employed to determine the ionic conductivity of the polymer membranes in the frequency range from 1 MHz to 1 Hz with an amplitude of 20 mV using a BioLogic VSP potentiostat. The EIS measurement was carried out in a two-electrode cell configuration where the membrane was sandwiched between two stainless-steel electrodes (SS) as ion-blocking electrodes (SS|SPE|SS). The temperature dependence of the Li^+ conductivity of each membrane was collected (at 30, 40, 60 and 80 °C).

To investigate the electrochemical stability window of the SPEs, the measurement was assessed using the linear sweep voltammetry (LSV) technique from open-circuit voltage (OCV) to 6 V at a scan rate of 0.1 mV s^{-1} at 60 °C. Then, an SS electrode played the part of a working electrode and Li metal was utilized as a reference and counter electrode (Li^0|SPE|SS).

The electrochemical tolerance of electrolytes against internal short-circuit failure (*i.e.*, lithium dendrite growth between electrodes) of the cells was evaluated by measuring the time evolution of voltage for a symmetrical cell (Li^0|SPE|Li^0, 2032-type coin) during repeated charge/discharge reactions, where the cell was cycled under a constant current density of 0.1 mA cm^{-2}.

The solid polymer electrolytes were prepared by a one-pot process and the standard solution casting technique. Initially, BPEI and PEGDMA (5 wt%) were added to a suitable solvent:ethanol. The solutions were stirred at room temperature until a homogenous solution was achieved. The lithium salt, LiTFSI, was added to the polymer solution, respecting the stoichiometric ratio (N : Li = 50), followed by stirring until a transparent solution was obtained. Then inorganic fillers were introduced into the solution with energetic stirring to avoid any settling phenomenon. Finally, AIBN was added with a concentration of 1 wt% with respect to the sum weight of methacrylate oligomers (PEGDMA).

Polymer solutions were cast in a Teflon mold. Two steps of thermal treatment were required to ensure crosslinking of PEGDMA and total evaporation of solvents at 70 °C, 15 h in a ventilated oven and 15 h under vacuum. The resulting composite s-IPN (Cs-IPN) SPEs, with a thickness between 100 and 200 μm, were directly placed in a glove box for further analysis.

NMR completes the information given by the physicochemical and electrochemical characterizations of the polymer electrolytes. Pulsed field gradient nuclear magnetic resonance (PFG-NMR) is a non-invasive method giving selective access to the diffusion coefficients (D) of the species of interest: in other words, the random translational motion that is driven by the internal kinetic energy of molecules or ions in solids or solutions.[35]

Results and discussion

The glass transition temperature (T_g) of BPEI was evaluated by differential scanning calorimetry (DSC) analysis in Fig. 8 (below) at around −37 °C. This low T_g does not allow mechanical integrity to be achieved. In order to overcome these blocking points, in previous work another nitrogenous polymer, poly(oxazoline), with a 42 °C T_g, was added to the PEI to mechanically reinforce the BEI-based electrolyte.[23] In the present work another macromolecular architecture, a so-called semi-interpenetrated network, is investigated thanks to PEG dimethacrylate and the addition of inorganic fillers. Before describing the results of these strategies (in the second part), it is important first to well characterize the BPEI. Infrared and ^{13}C NMR spectroscopy helped by DFT modeling were used to characterize the BPEI structure and to explore the several potential complexation sites for Li^+.

BPEI characterisation

Three types of amine coexist in BPEI: tertiary (N), secondary (NH) and primary (NH_2). In order to understand and describe the lithium-ion transport mechanism, a quantification of these different amine groups is required. The ^{13}C NMR spectrum of the commercially available BPEI is shown in Fig. 1. As mentioned, a highly branched PEI contains primary, secondary, and tertiary amine groups; following previous work,[15–17] the seven major ^{13}C peaks have been assigned according to the different combinations of amine nearest neighbors, as listed in Fig. 1.

As reported in Table 1, commercial BPEI is mainly composed of secondary amines (44.28%) and tertiary amines (35.84%) with around 20% of primary amines.

Thanks to the nitrogen atoms of the BPEI backbone, this polymer is capable of dissociating lithium salts, as reported in the literature.[36,37] Furthermore, its low glass transition temperature of about −40 °C permits high mobility of polymer chains and transport of lithium cations.

The experimental IR spectrum of the BPEI:LiTFSI mixture was collected (Fig. 3) to identify the Li-BPEI interactions through Li^+–amine interactions. The spectrum is complex, and it is difficult to identify the different types of amine in interaction with Li^+. To overcome this difficulty, DFT calculations

Table 1 ^{13}C NMR quantification of the amine units in BPEI

Amine type	Chemical structure	Proportion in BPEI (%)
Tertiary amines		35.84
Secondary amines		44.28
Primary amines		19.84

were performed to determine the most likely interaction sites for lithium cations with the polymer matrix and, for the so-obtained structures, theoretical IR spectra were generated (Fig. 2 and 3). Keeping in mind that, due to simplification of the polymers (reduced number of repetitive units compared to the experiment, the concentration of the different species such as LiTFSI cannot be considered), a frequency shift is possible. However, an experiment–simulation comparison must allow identification of the vibration bands, thus validating the interactions involved.

Three configurations were considered: Li^+ interacts with (i) a tertiary amine (Li–N), (ii) a secondary amine (Li–NH), or (iii) a primary amine (Li–NH_2) (Fig. 2). The three corresponding calculated spectra were then compared to the experimental

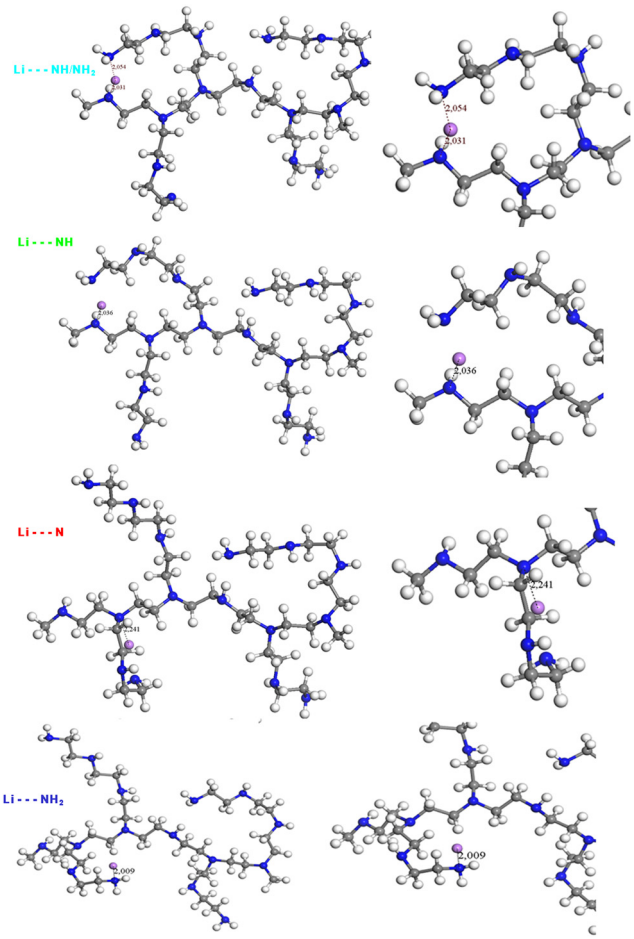

Fig. 2 Possible interactions between Li^+ and the different types of amines simulated by DFT. On the left, the global structure and on the right a zoomed-in picture of the interaction site are provided.

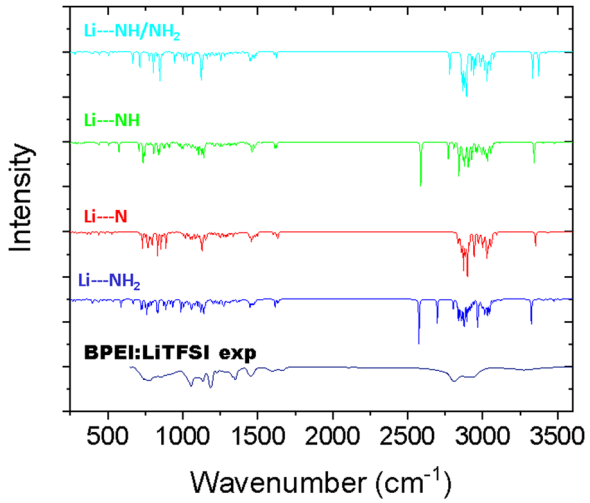

Fig. 3 Theoretical IR spectra deduced from the DFT calculations compared with the experimental one. The interactions involved in the models are always between Li^+ and N from amine.

spectrum (Fig. 3), as well as a configuration corresponding to a double interaction between NH and NH_2 (which corresponds to the configuration with the minimum energy, as observed in Table 2).

In Fig. 2, the main interaction distances between the amines and Li^+ have been reported and range from 2.0 (for interactions of Li^+ with NH and NH_2 groups) to 2.2 Å (for interactions of Li^+ with tertiary amine). As observed in the case of NH/NH_2, Li^+ can migrate to form a double interaction with primary and secondary amines with low distances. The energy values obtained for each configuration after geometric optimization are given in Table 2.

As observed from these values (Table 2), the most stable interaction is the interaction involving both NH and NH_2. The energy of the polymer in interaction with NH is very close while that in which the interaction occurs with N or NH_2 alone is weaker. It follows that the most plausible interaction is between NH or NH/NH_2. These results are consistent with the evolution of the distances between Li^+ and polymer observed in Fig. 2. It should, however, be kept in mind that the DFT calculations are performed at 0 K and that the temperature can have an impact on the interaction site as well as the dynamics of the polymer or the cation.

Another question is whether Li^+ is interacting with the counter-ion $TFSI^-$ and is in interaction with the polymer or not. Calculations considering the global Li-TFSI have been performed and the resulting configuration (−2150.3072605 Ha) seems to confirm that Li^+ is probably in double interaction with the polymer and $TFSI^-$ (see Fig. 4).

To go further, a comparison between experimental and theoretical IR spectra should help to clarify the preferential interaction site. We can see in Fig. 3 that the theoretical IR spectra obtained for configurations involving NH_2 and NH present a fine and intense peak at 2600 cm^{-1}. This peak does not, however, appear in the experimental spectra.

This peak corresponds to the C–H bond near a nitrogen atom, strongly disturbed by the presence of the lithium cation in interaction with the secondary or primary amine. We can therefore exclude these configurations and this type of interaction. On the other hand, the experimental spectrum clearly presents more similarities with the interactions of the first situation. Moreover, the case of chemisorption, where a Li atom substitutes a hydrogen atom and becomes chemically attached to the polymer chain, appears implausible due to the ionic conductivity (discussed below), showing that the Li^+ ions are free to move within the BPEI and that they are not directly bound to the polymer. The case retained is therefore an interaction between Li^+ and the polymer *via* the tertiary amines. In conclusion, the configuration with interaction through the NH/NH_2 and N groups of the polymer seems to be the most probable. The ionic conductivity of such an SPE is now interrogated and measured and discussed in the next part.

Table 2 Energy values extracted from the structures containing interactions between polymer and Li^+ investigated by DFT calculations

Interaction between polymer and Li^+	Energy value (Ha)
NH/NH_2	−2150.0505422
N	−2150.0291912
NH	−2150.0469645
NH_2	−2150.0103548

Ionic conductivity

Ionic conductivity is one of the main parameters for application of an SPE. It is closely related to the diffusion of cations and anions in the electrolyte. When doped with LiTFSI, BPEI shows an ionic conductivity following non-linear Vogel–Tammann–Fulcher (VTF) behaviour with temperature, meaning that ion mobility is activated by segmental motion of polymer chains. Ionic conductivity has been measured between 25 and 80 °C with values from 2.7×10^{-7} to 3.5×10^{-5} S cm^{-1}, as reported in Fig. 5, with corresponding Nyquist plots. Optimal salt concentration has been studied[7] and 10 wt% of LiTFSI in BPEI represents the best compromise between the number of charged species and polymer chain mobility with an increased T_g (as shown in Fig. SI1, ESI†).

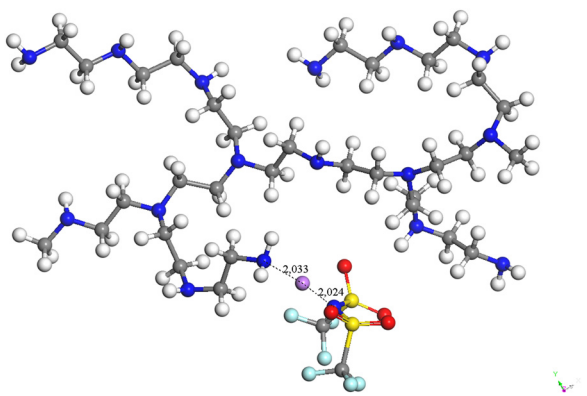

Fig. 4 Structure of LiTFSI in interaction with the polymer (obtained from DFT calculations).

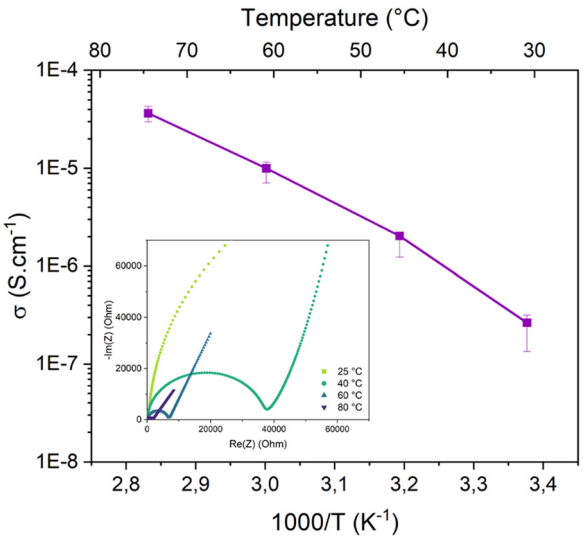

Fig. 5 BPEI ionic conductivity as a function of temperature.

If ionic conductivity is an important parameter closely related to the diffusion of cations and anions in the electrolyte, measurement performed by impedance spectroscopy measures only a global contribution which corresponds to the sum of the contributions of all the charged species. However, only the contribution of the Li^+ cation participates in the proper functioning of the battery. With PFG-NMR performed at the frequency of lithium (^{7}Li NMR) and fluorine (^{19}F NMR), we have access to the diffusion coefficients (D) of the species of interest; in other words, to the mobility of cations and anions, respectively. The selective measurement of the diffusion coefficients of Li and F present in the $TFSI^-$ anion makes it possible to account for the contribution of each species to global conductivity and thus to calculate the transport number. The NMR technique cannot distinguish isolated ions from ion pairs or weakly dissociated clusters, which tends to lead to an error in the estimation of the conductivity from the diffusion coefficients.[38,39]

The diffusion coefficients (denoted D^+ for the diffusion coefficient of the cation and D^- for the diffusion coefficient of the anion), which are used to evaluate the mobility of the ions in a system, can also be used to calculate the transport number ($t_{RMN}{}^+$), which is a measure of cation mobility relative to anion mobility (using eqn (1) where z^+ and z^- are the charges on the cation and anion, respectively).[40,41] This method of measuring the transport number works best in dilute systems because it assumes that ion–ion interactions are negligible and therefore only considers certain associated species (it considers only isolated ions).[41] Therefore, the transport numbers are related by: $t^- = 1 - t^+$. A cation transport number of 1 should overcome the problems associated with concentration gradients.[42]

$$t_{RMN}{}^+ = \frac{z^+D^+}{z^+D^+ - z^-D^-} \quad (1)$$

NMR spectroscopy was used to obtain the diffusion coefficients of Li and F species in our electrolyte. At 80 °C, the coefficients of Li and F were measured in the BPEI electrolyte (25 000 g mol^{-1}): LiTFSI (10 wt%) at 1.64×10^{-12} and 5.87×10^{-12} m^2 s^{-1}, respectively (Fig. 6a). A low transport number of 0.22 was deduced, suggesting that the Li^+ cation is slowed down, probably by interactions with the polymer but continues to diffuse into our polymer matrix. The BPEI:LiTFSI electrolyte shows rather low diffusion coefficients compared to a PEO-based electrolyte ($D_{Li^+} = 7 \times 10^{-12}$ m^2 s^{-1} and $DTFSI^- = 3 \times 10^{-11}$ m^2 s^{-1} [43]) but has a t^+ transport number equivalent to the oxygenated system.

Diffusion coefficient measurements were performed on a more concentrated LiTFSI system (Fig. 6a) of 40 wt%. In this case, a clear decrease in the diffusion coefficients is observed with coefficients of 3.54×10^{-13} m^2 s^{-1} for Li^+ and 1.88×10^{-12} m^2 s^{-1} for $TFSI^-$ and a low transport number is reached of 0.16. These results highlight a sharp decrease in the

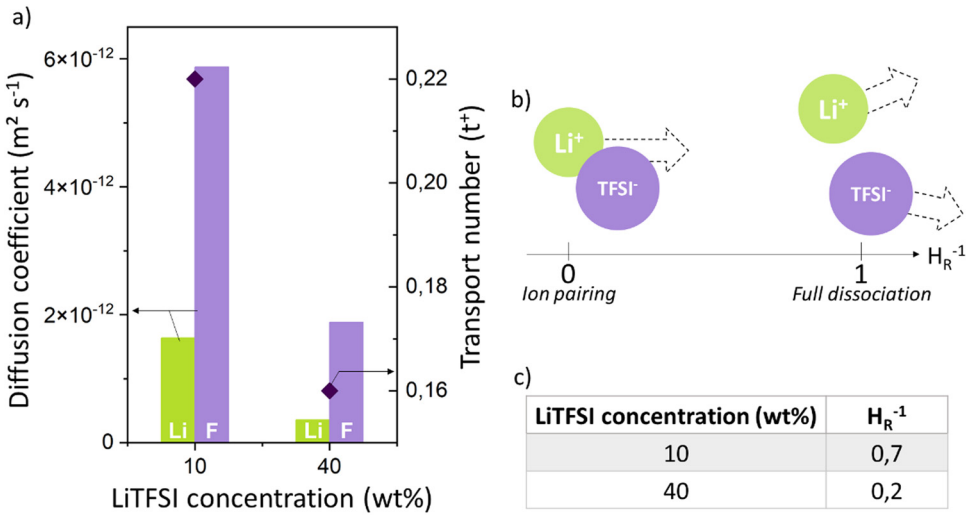

LiTFSI concentration (wt%)	H_R^{-1}
10	0,7
40	0,2

Fig. 6 (a) Diffusion coefficients Li and F and transport numbers for a BPEI25000:LiTFSI electrolyte at different salt concentrations. (b) Description of the impact of the inverse Haven ratio tending to 0 or tending to 1. (c) Inverse Haven ratio (H_R^{-1}) for 10 and 40 wt% of LiTFSI.

transport performance of charged species with increasing salt concentration.

However, it should be noted that differences between the transport numbers calculated with GFP-NMR and the various electrochemical techniques exist and can be explained by the dissociation of ionic species. As GFP-NMR does not distinguish between dissociated and undissociated species, the transport numbers reported by this technique tend to be artificially higher than those determined by electrochemical methods, since the motions of neutral pairs, dissociated ions, and charged groups are averaged.[44,45] Conversely, ionic conductivity measured by impedance, for example, accounts for charge diffusion and not directly for ion diffusion.[46–48] In samples where the transport numbers obtained by NMR spectroscopy and electrochemical methods are similar, the dissociation of ionic species is almost complete. Otherwise, a dissociation ratio called the inverse Haven ratio (H_R^{-1}), shown in eqn (2), is used to describe the extent to which ionic species are dissolved in a sample, with 1 indicating perfect dissociation and 0 indicating no dissociation, as illustrated in Fig. 6b.[44] A ratio lower than 1 suggests that not all ions contribute to the conductivity and that there is a correlation between the movements of cations and anions. The inverse Haven ratio is used for the study of correlation effects and therefore of the microscopic diffusion mechanism, and is calculated from the ionic conductivity measured by impedance as well as from the diffusion coefficients of the ions obtained by PFG-NMR, considering the salt concentration by using the Nernst–Einstein relation:[49]

$$H_R^{-1} = \frac{\sigma_{ion}}{\sigma_+^{self} + \sigma_-^{self}} \quad (2)$$

where σ_{ion} is the ionic conductivity measured by impedance, and σ_+^{self} and σ_-^{self} are the ionic conductivity calculated from the diffusion coefficients determined by PFG-NMR (eqn (3) and (4), respectively):

$$\sigma_+^{self} = \frac{C_{salt}F^2}{RT}D^+ \quad (3)$$

$$\sigma_-^{self} = \frac{C_{salt}F^2}{RT}D^- \quad (4)$$

where C_{salt} is the molar salt concentration, F is the Faraday constant, and D^+ and D^- are the diffusion coefficients of lithium and fluorine, respectively.

The inverse Haven ratios for our electrolytes are reported in Fig. 6c. We note that in the more concentrated ionic electrolytes, H_R^{-1} decreases and tends to 0, reflecting the presence of ion-pair diffusion that does not contribute to the conductivity. At high salt concentration, ion–ion correlations are not negligible and can strongly affect the ionic conductivity.[50–52] Such phenomena have been observed in various ion-conducting oxide glasses, such as Na or K for example,[53] where the ion-pair associations contribute to the diffusion process but not to the ionic conductivity, which is strongly reduced.[51]

Once the charge transport mechanism in this new BPEI-based electrolyte was better understood, we experimentally investigated its capacity to transport lithium. As mentioned above, its low T_g does not allow sufficient mechanical strength. This has therefore been reinforced by preparing semi-interpenetrating polymer electrolyte membranes, Cs-IPNs, and adding mineral fillers.

BPEI-based Cs-IPN polymer electrolytes (with and without fillers)

Semi-interpenetrating polymer electrolyte membranes (Cs-IPNs) result from the crosslinking of dimethacrylated PEO

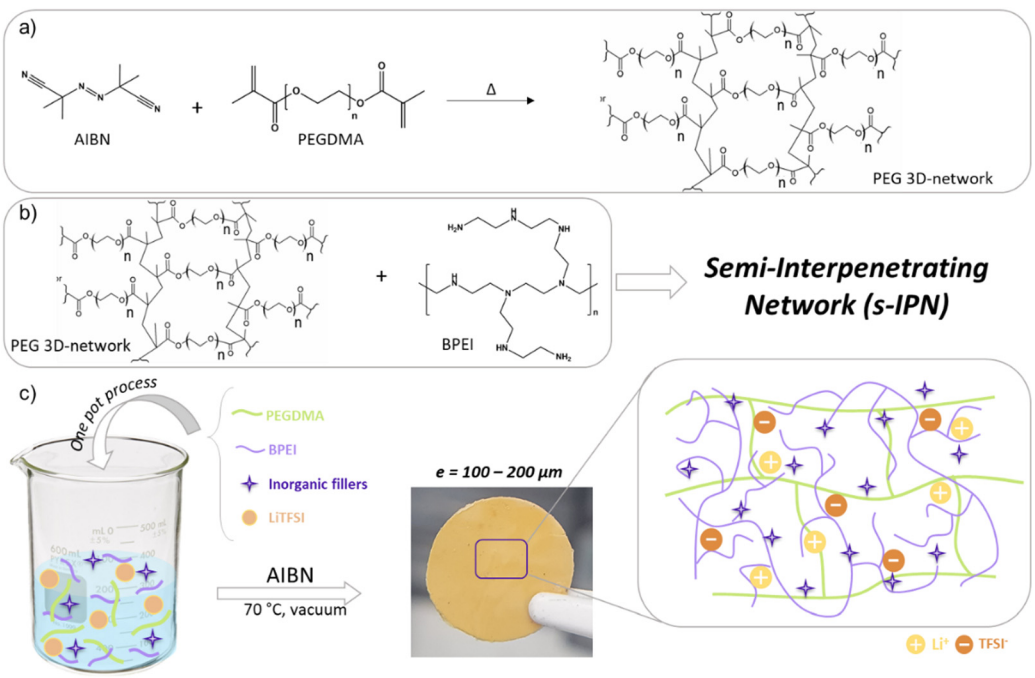

Fig. 7 Typical route for the synthesis of BPEI-based Cs-IPN polymer electrolytes with (a) the formation of a crosslinked structure with AIBN. (b) The chemical structures of polymers composing the s-IPN and (c) the process and SPE obtained.

(PEGDMA) in which BPEI chains are tangled, and LiTFSI and inorganic fillers with nanometric size are sequestered, as shown schematically in Fig. 7b. The good compatibility between PEO and PEI repetitive units comes from the ability to form hydrogen bonds between the N–H bond of PEI and the oxygen atom of PEO.

The polymer blend was initially diluted in ethanol to homogeneously incorporate the other components into a Teflon mold and produce a membrane with tailored structural/physicochemical characteristics by a casting process. Under heating, the thermal decomposition of AIBN generated free radicals able to initiate the polymerization of bifunctional crosslinker PEGDMA (Fig. 7a). We noted that crystallization of the PEO chain was avoided by crosslinking and the small amount of PEGDMA (5 wt%) was sufficient to shape a self-standing film. In the end, flexible and handleable films were obtained with a thickness between 100 and 200 μm (Fig. 7c).

The glass transition temperature (T_g) was evaluated by differential scanning calorimetry (DSC) analysis and the resulting thermograms are shown in Fig. 8b. DSC measurements were performed on the series of polymer electrolytes from bulk BPEI to s-IPNs alone and doped with inorganic fillers Cs-IPN. The corresponding T_g values are also listed on the thermograms and correspond to the midpoint of the heat capacity change during the transition from glassy to rubbery state. The analyses evidenced unchanged T_g values when a crosslinked network or inorganic fillers were incorporated. All Cs-IPN electrolytes show a low T_g of about −35 °C, permitting high segmental relaxation and easy transport of lithium ions. It can be deduced from the DSC studies that all membranes were in the rubbery state at ambient temperature and were composed of one single homogeneous amorphous phase. So, PEGDMA does not bring about crystallinity and allows high mobility for polymer chains and lithium cations. Furthermore, no appreciable change in T_g values has occurred due to the addition of inorganic fillers into the s-IPN membranes. This suggests that the presence of ceramic nanopowders has not drastically changed the main-chain dynamics governing the glass transition of the material.

The temperature-dependent ionic conductivity of the Cs-IPN electrolyte compared with an s-IPN electrolyte was determined

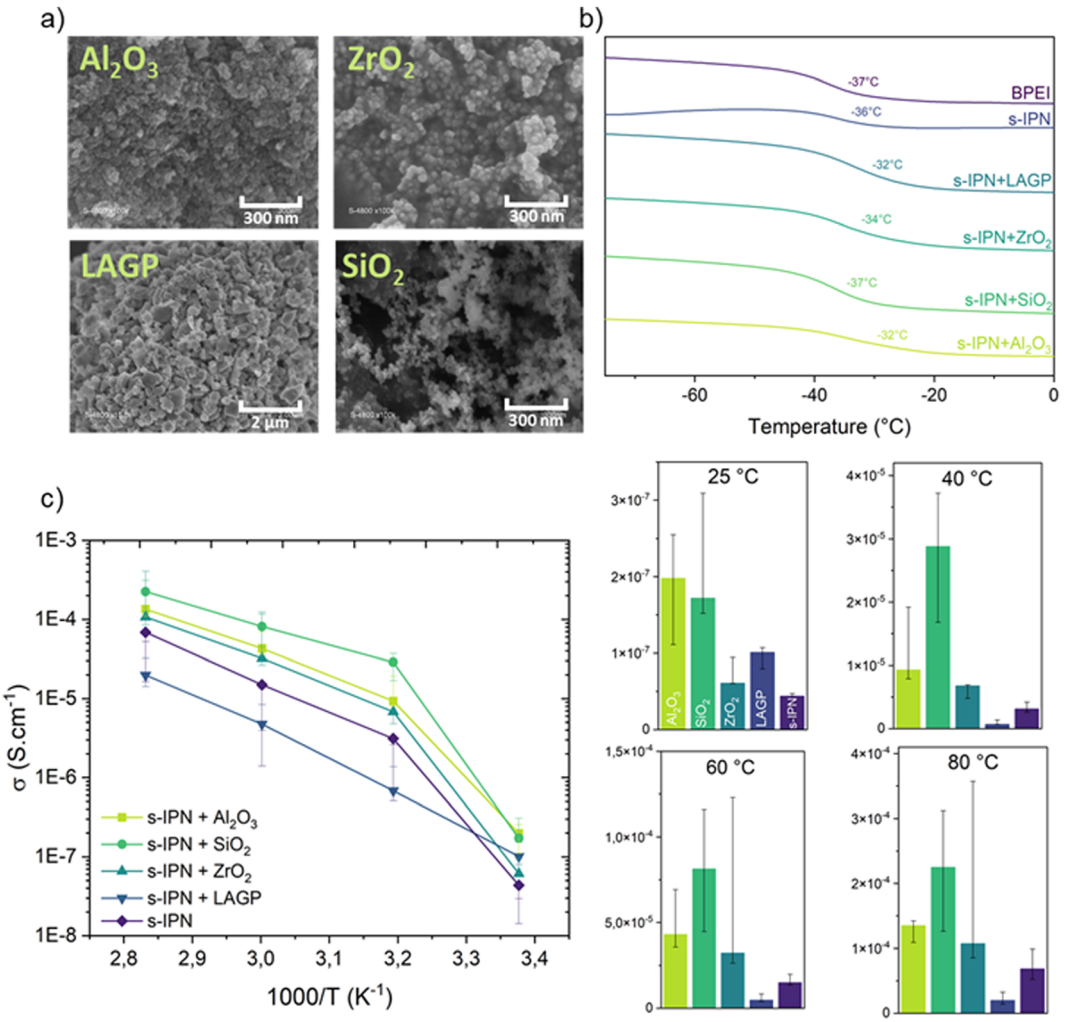

Fig. 8 (a) SEM images of ceramic nanopowders. (b) Thermograms with T_g shown and (c) ionic conductivity of s-IPN and Cs-IPN SPEs at different temperatures.

from EIS measurements, as presented in Fig. 8c. As expected, the ionic conductivity increased with temperature for all the tested samples due to the improved mobility of Li^+ through the membrane. Moreover, the ion mobility can decrease according to the content of crosslinking agent, here PEGDMA. This is evidenced by the continuously reducing ionic conductivity when the content of PEGDMA is increased from 2 to 10 wt% in Fig. SI2 (ESI†). For high PEGDMA content, the crosslinking density of the formed polymer networks can reduce the movement of BPEI segments, resulting in decreased ionic conductivity. However, for the semi-interpenetrating membrane containing 5 wt% of PEGDMA, the small amount of crosslinking agent is sufficient to obtain a self-standing film without excessively stiffening the material, resulting in a reduced ionic conductivity at room temperature and a slightly improved one above 40 °C (3×10^{-6} S cm^{-1}, as shown in Fig. SI2, ESI†) compared with BPEI alone (2×10^{-6} S cm^{-1}). Thus, SPE containing 5 wt% of PEGDMA was used as the s-IPN electrolyte for the addition of fillers. As illustrated in Fig. 8b and c, the ionic conductivity of the Cs-IPN electrolyte is observed to be higher than that of the s-IPN electrolyte, except for LAGP, over a wide range of temperature. The highest conductivities are obtained with the addition of SiO_2 nanopowder reaching 2.2×10^{-4} S cm^{-1} at 80 °C – three times the value without any filler (7×10^{-5} S cm^{-1}). At room temperature, a maximum ionic conductivity of 2×10^{-7} S cm^{-1} is detected with the addition of Al_2O_3 nanopowder, comparable to an s-IPN formed with free PEO chains and PEGDMA.[12] ZrO_2 gives the next highest enhancement in conductivity followed by LAGP over the entire temperature range studied.

Only for LAGP, the popular sodium superionic conductor ceramic discovered by Goodenough *et al.* approximately four decades ago[54] and used as solid electrolyte, is a reduced ionic conductivity at any temperature observed. Its Li^+ transport mechanism is different from those found in SPEs. In LAGP during ionic transport, Li^+ moves from site to site composed of triangular void areas spanned by three oxygen atoms within the crystalline structure.[55] This open and stable structure can provide a three-dimensional channel for the isotropic diffusion of alkali ions with a low activation energy, which makes this NASICON-type crystal a favourable material for solid-sate electrolytes. Despite a high bulk conductivity of about 10^{-4} S cm^{-1} at RT,[56] the introduction of nanopowder in the s-IPN structure does not improve the ionic transport of the overall Cs-IPN membrane. A percolating path for Li^+ is probably required to attain high ionic conductivity at ambient temperature. This Cs-IPN needs to be optimized and studied further, as a totally different transport mechanism is involved.

The enhancement in ionic conductivity when fillers are introduced into the polymer matrix is not fully understood. Numerous studies about hybrid PEO-based SPEs suggest controverted explanations. By definition, an improvement in conductivity can only be caused by an increase in the number of charge carriers or an augmented mobility. The non-linear VTF-type behaviour indicated in the $\log(\sigma)$ *versus* $1000/T$ plots suggests that, even in the composite polymer electrolyte, ionic transport takes place predominantly by the same mechanism as that in the filler-free electrolyte, namely by the segmental motion of the polymer chains. Moreover, according to the DSC results, the Cs-IPN electrolyte appears to behave similarly to the s-IPN membrane, suggesting that the contribution to conductivity enhancement from the segmental flexibility of the PEO chains is essentially unaffected by the addition of the filler grains. No strong interactions seem to occur between the polymer/salt complex and the ceramic particles. In the literature, NMR studies on PEO:$LiClO_4$:nanosized Al_2O_3, TiO_2 and SiO_2 fillers have demonstrated that the increased ionic conductivity is not attributable to a corresponding increase in polymer segmental motion, but is more likely due to a weakening of the polyether–cation interaction induced by the nanoparticles.[18] Authors have suggested that the sites on the surface of the ceramic particles may compete with the basic oxygens on the PEO chains to form complexes with the lithium cations, thereby promoting salt dissociation.[57] The same group has reported enhancement in the conductivity in the $(PEO)_{20}$:-$LiCF_3SO_3$ system due to the addition of nanosized Al_2O_3 particles.[20] They have attributed the mechanism of enhancement to different types of interactions existing between the chemical functions at the surface of fillers with the salt species as electrostatic interactions[58] and the formation of Lewis acid/base interactions leading to ionic dissociation and generating more cations.[20]

The thermal stability of the samples was assessed by thermogravimetric analysis (TGA). The resulting thermograms are shown in Fig. 9a. A high-temperature single-step weight loss is shown, which accounts for the homogeneity of the semi-interpenetrating solid electrolytes with noticeable deflection only above 300 °C. The thermal stability of the samples, corresponding to the temperature where 5% of weight is lost, is shown in the yellow frame in Fig. 9a. The $T_{5\%}$ values for all studied s-IPNs approach or surpass 300 °C, indicating that the polymer electrolytes are highly stable for use up to very high temperatures. The residues recovered at 450 °C correspond to the ceramic fillers incorporated in the polymer electrolyte known for their high thermal stability.[59] It can be seen that the Cs-IPN-containing ZrO_2 nanopowder exhibits the highest thermal stability to about 320 °C. Once again, LAGP has a negative impact on the properties of s-IPN SPE, with a lower degradation temperature of about 290 °C.

The electrochemical stability window (ESW) is another fundamental parameter that is required for further lithium plating and stripping processes. The ESW of Cs-IPN polymer electrolytes containing different types of filler was evaluated by linear sweep voltammetry (LSV), as shown in Fig. 9b. For comparison, the LSV curve of a membrane without the addition of inorganic nanoparticles was also plotted. During the anodic sweep towards higher potential values, the onset of a current increase at approximatively 3.5 V *vs.* Li^+/Li is shown by the yellow frame in Fig. 9b. At this voltage the decomposition (oxidation) of the electrolyte is likely to start. Progressively, the current increases and becomes steeper at 4 V. The addition of fillers does not cause a significant change in electrochemical stability of s-IPN

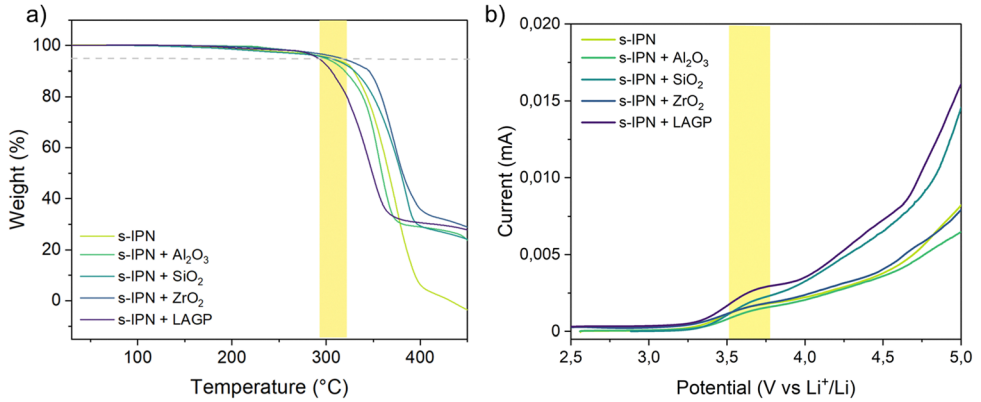

Fig. 9 (a) TGA analysis and (b) LSV measurements of s-IPN and Cs-IPN SPEs.

SPEs, in agreement with the results obtained for thermal properties.

To evaluate the compatibility of Cs-IPN with electrochemical systems, the long-term lithium plating/stripping performance of an Li|Cs-IPN SPE|Li symmetric coin cell was investigated at a current density of J = 0.1 mA cm^{-2} at 80 °C. All the cells were cycled with 30 min of Li-plating and 30 min of Li-stripping. The galvanostatic cycling profiles are shown in Fig. 10. The negative voltage refers to lithium plating, and the positive voltage refers to lithium stripping.

Preliminary studies of s-IPN without any fillers revealed an asymmetrical response and a rapid polarization of the cell after a few cycles only in one side, during lithium stripping, as observed in Fig. 10. In these conditions, the side of the membrane in contact with air during the process is the negative side, whereas the side in contact with the Teflon mold is the positive side. Depending on the method of placement of the membrane in the chemical cell, a big difference in polarization is observed: if the side of the membrane which was in contact with the Teflon mold is on the side of the working electrode, an asymmetric polarization is observed during stripping or plating, demonstrating the effect of SPE surface morphology on stability. It demonstrates the effect of SPE surface morphology on the stability. The quality of this surface probably has an influence on the lithium electrode/SPE interface and consequently on the resistance of the cell. Surprisingly, whatever nanopowder is added, totally identical behaviour is observed. A tremendous decrease in polarization and very stable cycling over a hundred hours are shown in Fig. 10. For all fillers, Al_2O_3, SiO_2, ZrO_2 and LAGP, the voltage remains between 0.05 and 0.09 V after 50 hours, indicating that the interface between the Li anode and Cs-IPN SPE is stable. Extended symmetric cycling has been achieved and the example of the SiO_2-IPN SPE polarization test over 250 h is given in ESI† (Fig. SI3). This result suggests that BPEI-based Cs-IPNs show excellent compatibility with an Li anode.

Repetitive cycling may form lithium dendrites piercing the polymer electrolyte, which will result in sudden and anarchic changes in voltage during cycling.[60,61] Therefore, changes in voltage over time can be used to follow the ability of the electrolyte membrane to inhibit dendrite growth. Here, the overpotential of the Li^0|Cs-IPN SPE|Li^0 cell remains stable even after 200 h, indicating that the interface between the SPE and

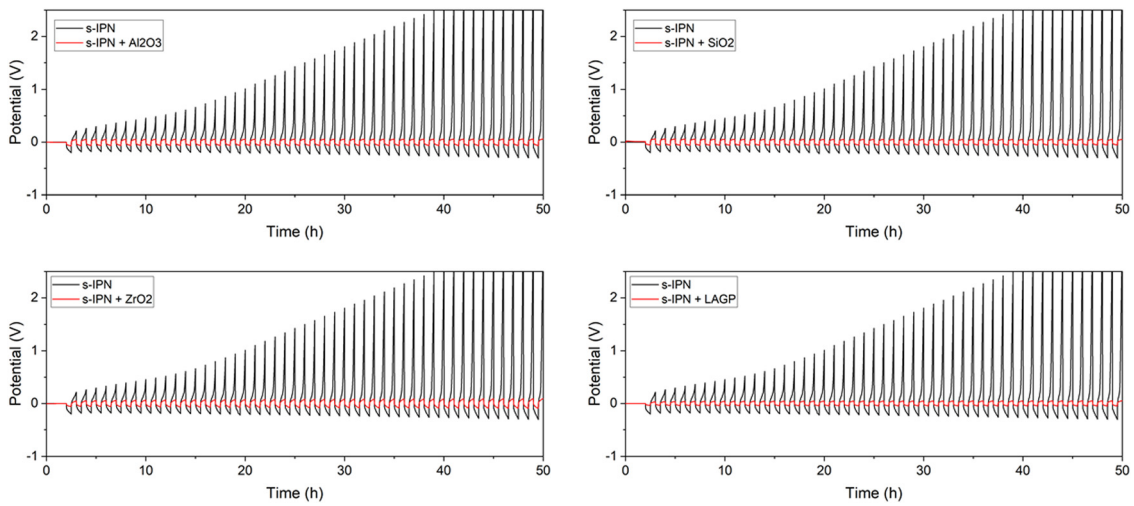

Fig. 10 Polarization test of S-IPN (black) and Cs-IPN (red).

lithium metal is stable, without any degradation. The uniformly dispersed fillers provide good cycle stability and long cycle life.

Conclusions

Nitrogen-rich polymers (NRPs), especially poly(ethyleneimine) (PEI), are still poorly explored as solid polymer electrolytes (SPEs) for Li-ion all-solid-state batteries. In this study we selected BPEI polymer to explore its properties as an SPE.

By comparing IR experimental and DFT simulated spectra, we determined that for BPEI, interactions exist between the Li^+ cation and the various amines present on the polymer chains with a privileged interaction with the tertiary amine. Thanks to NMR-PFG, we were able to show that the diffusion coefficient of F is greater than that of Li, meaning that the TFSI anion moves more quickly and easily in the BPEI-based matrix than the Li^+ ion. A BPEI system containing 10 wt% LiTFSI has a transport number of 0.22, which is comparable to an equivalent system containing PEO. When the salt content is increased in the BPEI SPE, the diffusion coefficients and the transport number decrease, and thermally we also observe an increase in T_g. We can explain these phenomena thanks to the inverse Haven ratio (HR^{-1}), which makes it possible to account for ion–ion interactions in the system. Here, using 10% of LiTFSI in BPEI, HR^{-1} tends towards 1, illustrating good ion dissociation.

To improve the mechanical properties of the BPEI electrolyte (low T_g), we combined it with PEGDMA in a network. The addition of a small amount of crosslinker, 5 wt% of PEGDMA, provides sufficient mechanical strength to obtain a self-supporting and easy-to-handle film, which represents a good compromise between mechanical properties and ionic conductivity.

During polarization tests, the studied SPE exhibited strong polarization during plating or during stripping. After the addition of nanosized inorganic fillers (Al_2O_3, SiO_2, ZrO_2 or LAGP), the electrochemical properties were strongly improved, without, at this stage, a clear explanation. The best ionic conductivities were obtained for a system composed of SiO_2, with 3×10^{-5} S cm^{-1} at 40 °C (*vs.* 4×10^{-6} S cm^{-1} for a PEO-based s-IPN[12]). The next step is to confirm that this new SPE could be efficient in full cells. Experiments on the cycling of an Li|SiO_2-IPN SPE|$LiFePO_4$ full cell are planned in the next study.

Conflicts of interest

There are no conflicts to declare.

Acknowledgements

The authors would like to acknowledge the "Agence Nationale de la Recherche et de la Technologie (ANRT)" and the company Renault Group for the financial support. The authors gratefully acknowledge the French National Research Agency (project Labex STORE-EX, ANR-10-LABX-76-01) and the help of V. Seznec in the LAPG delivering. Financial support from the IR INFRANALYTICS FR2054 for conducting the research is gratefully acknowledged.

References

1 A. Jana and R. E. García, Lithium dendrite growth mechanisms in liquid electrolytes, *Nano Energy*, 2017, **41**, 552–565.
2 D. E. Fenton, J. M. Parker and P. V. Wright, Complexes of alkali metal ions with poly(ethylene oxide), *Polymer*, 1973, **14**, 589.
3 L. R. A. K. Bandara, M. A. K. L. Dissanayake and B. E. Mellander, Ionic conductivity of plasticized(PEO)–$LiCF_3SO_3$ electrolytes, *Electrochim. Acta*, 1998, **43**, 1447–1451.
4 B. Sun, J. Mindemark, K. Edström and D. Brandell, Realization of high performance polycarbonate-based Li polymer batteries, *Electrochem. Commun.*, 2015, **52**, 71–74.
5 T. Okumura and S. Nishimura, Lithium ion conductive properties of aliphatic polycarbonate, *Solid State Ion*, 2014, **267**, 68–73.
6 D. Mouraliraman, *et al.*, Thermally Stable PVDF-HFP-Based Gel Polymer Electrolytes for High-Performance Lithium-Ion Batteries, *Nanomaterials*, 2022, **12**, 1056.
7 L. Artigues, B. T. Benkhaled, V. Chaudoy, L. Monconduit and V. Lapinte, Two routes for N-rich solid polymer electrolyte for all-solid-state lithium-ion batteries, *Solid State Ion*, 2022, **388**, 116086.
8 C. S. Harris, D. F. Shriver and A. Ratner, Complex Formation of Poly(ethylenimine) with Sodium Triflate and Conductivity Behavior of the Complexes Introduction The potential application of solvent-free polymer-salt, *Catal. Enzyme Action*, 1986, **19**, 3570.
9 C. S. Harris, M. A. Ratner and D. F. Shriver, Ionic Conductivity in Branched Polyethylenimine-Sodium Trifluoromethanesulfonate Complexes. Comparisons to Analogous Complexes Made with Linear Polyethylenimine, *Macromolecules*, 1987, **20**, 1778–1781.
10 L. J. Goujon, *et al.*, Flexible solid polymer electrolytes based on nitrile butadiene rubber/poly(ethylene oxide) interpenetrating polymer networks containing either LiTFSI or EMITFSI, *Macromolecules*, 2011, **44**, 9683–9691.
11 S. Oh, D. W. Kim, C. Lee, M. H. Lee and Y. Kang, Poly(vinylpyridine-*co*-styrene) based in situ cross-linked gel polymer electrolyte for lithium-ion polymer batteries, *Electrochim. Acta*, 2011, **57**, 46–51.
12 G. Homann, L. Stolz, M. Winter and J. Kasnatscheew, Elimination of 'Voltage Noise' of Poly (Ethylene Oxide)-Based Solid Electrolytes in High-Voltage Lithium Batteries: Linear versus Network Polymers, *iScience*, 2020, **23**, 101225.
13 J. Jiang, H. Pan, W. Lin, W. Tu and H. Zhang, UV-induced semi-interpenetrating polymer electrolyte membrane for elevated-temperature all-solid-state lithium-ion batteries, *Mater. Chem. Phys.*, 2019, **236**, 121781.
14 C. W. Nan, L. Fan, Y. Lin and Q. Cai, Enhanced ionic conductivity of polymer electrolytes containing nanocomposite SiO2 particles, *Phys. Rev. Lett.*, 2003, **91**, 266104.
15 J. E. Weston and B. C. H. Steele, Effects of inert fillers on the mechanical and electrochemical properties of lithium salt-poly(ethylene oxide) polymer electrolytes, *Solid State Ion*, 1982, **7**, 75–79.

16 S. Das and A. Ghosh, Ion conduction and relaxation in PEO-LiTFSI-Al2O3 polymer nanocomposite electrolytes, *J. Appl. Phys.*, 2015, **117**, 174103.
17 C. C. Tambelli, *et al.*, Characterisation of PEO–Al2O3 composite polymer electrolytes, *Electrochim. Acta*, 2002, **47**, 1677–1682.
18 S. H. Chung, *et al.*, Enhancement of ion transport in polymer electrolytes by addition of nanoscale inorganic oxides, *J. Power Sources*, 2001, **97–98**, 644–648.
19 Y. W. Chen-Yang, H. C. Chen, F. J. Lin and C. C. Chen, Polyacrylonitrile electrolytes: 1. A novel high-conductivity composite polymer electrolyte based on PAN, $LiClO_4$ and α-Al_2O_3, *Solid State Ion*, 2002, **150**, 327–335.
20 F. Croce, *et al.*, Role of the ceramic fillers in enhancing the transport properties of composite polymer electrolytes, *Electrochim. Acta*, 2001, **46**, 2457–2461.
21 I. W. Cheung, *et al.*, Electrochemical and solid state NMR characterization of composite PEO-based polymer electrolytes, *Electrochim. Acta*, 2003, **48**, 2149–2156.
22 S. Ramesh and L. C. Wen, Investigation on the effects of addition of SiO2 nanoparticles on ionic conductivity, FTIR, and thermal properties of nanocomposite PMMA-$LiCF_3SO_3$-SiO_2, *Ionics*, 2010, **16**, 255–262.
23 C. Capiglia, P. Mustarelli, E. Quartarone, C. Tomasi and A. Magistris, Effects of nanoscale SiO_2 on the thermal and transport properties of solvent-free, poly(ethylene oxide) (PEO)-based polymer electrolytes, *Solid State Ion*, 1999, **118**, 73–79.
24 G. B. Appetecchi, *et al.*, Hot-pressed, dry, composite, PEO-based electrolyte membranes: I. Ionic conductivity characterization, *J. Power Sources*, 2003, **114**, 105–112.
25 P. Johansson, M. A. Ratner and D. F. Shriver, The influence of inert oxide fillers on poly(ethylene oxide) and amorphous poly(ethylene oxide) based polymer electrolytes, *J. Phys. Chem. B*, 2001, **105**, 9016–9021.
26 Y. Tominaga and K. Yamazaki, Fast Li-ion conduction in poly(ethylene carbonate)-based electrolytes and composites filled with TiO_2 nanoparticles, *Chem. Commun.*, 2014, **50**, 4448–4450.
27 B. Scrosati, F. Croce and L. Persi, Impedance Spectroscopy Study of PEO-Based Nanocomposite Polymer Electrolytes, *J. Electrochem. Soc.*, 2000, **147**, 1718.
28 F. Croce, L. Settimi and B. Scrosati, Superacid ZrO_2-added, composite polymer electrolytes with improved transport properties, *Electrochem. Commun.*, 2006, **2**, 364–368.
29 A. D'Epifanio, *et al.*, Metallic-lithium, LiFePO4-based polymer battery using PEO–ZrO_2 nanocomposite polymer electrolyte, *J. Appl. Electrochem.*, 2004, **34**, 403–408.
30 F. S. Fiory, *et al.*, PEO based polymer electrolyte lithium-ion battery, *J. Eur. Ceram. Soc.*, 2004, **24**, 1385–1387.
31 F. Croce, S. Sacchetti and B. Scrosati, Advanced, lithium batteries based on high-performance composite polymer electrolytes, *J. Power Sources*, 2006, **162**, 685–689.
32 M. R. Johan and L. B. Fen, Combined effect of CuO nanofillers and DBP plasticizer on ionic conductivity enhancement in the solid polymer electrolyte PEO–$LiCF_3SO_3$, *Ionics*, 2010, **16**, 335–338.
33 A. Karmakar and A. Ghosh, Poly ethylene oxide (PEO)-LiI polymer electrolytes embedded with CdO nanoparticles, *J. Nanopart. Res.*, 2011, **13**, 2989–2996.
34 J. Kumar, S. J. Rodrigues and B. Kumar, Interface-mediated electrochemical effects in lithium/polymer-ceramic cells, *J. Power Sources*, 2010, **195**, 327–334.
35 W. S. Price, Pulsed-Field Gradient Nuclear Magnetic Resonance as a Tool for Studying Translational Diffusion: Part 1. Basic Theory, *Concepts Magn. Reson.*, 1997, **9**, 277–357.
36 J. L. Paul, C. Jegat and J. C. Lassègues, Branched poly(ethyleneimine)-CF_3SO_3Li complexes, *Electrochim. Acta*, 1992, **37**, 1623–1625.
37 I. B. Pehlivan, P. Georen, R. Marsal, C. G. Granqvist and G. A. Niklasson, Ion conduction of branched polyethyleneimine-lithium bis(trifluoromethylsulfonyl) imide electrolytes, *Electrochim. Acta*, 2011, **57**, 201–206.
38 B. Sun, *et al.*, Ion transport in polycarbonate based solid polymer electrolytes: experimental and computational investigations, *Phys. Chem. Chem. Phys.*, 2016, **18**, 9504–9513.
39 F. U. Shah, O. I. Gnezdilov, R. Gusain and A. Filippov, Transport and Association of Ions in Lithium Battery Electrolytes Based on Glycol Ether Mixed with Halogen-Free Orthoborate Ionic Liquid, *Sci. Rep.*, 2017, **7**, 1–13.
40 K. D. Fong, *et al.*, Ion Transport and the True Transference Number in Nonaqueous Polyelectrolyte Solutions for Lithium Ion Batteries, *ACS Cent. Sci.*, 2019, **5**, 1250–1260.
41 J. Mindemark, M. J. Lacey, T. Bowden and D. Brandell, Beyond PEO—Alternative host materials for Li^+-conducting solid polymer electrolytes, *Prog. Polym. Sci.*, 2018, **81**, 114–143.
42 N. Verdier, *et al.*, Cross-Linked Polyacrylonitrile-Based Elastomer Used as Gel Polymer Electrolyte in Li-Ion Battery, *ACS Appl. Energy Mater.*, 2020, **3**, 1099–1110.
43 R. J. Messinger, T. Vu Huynh, R. Bouchet, V. Sarou-Kanian and M. Deschamps, Magic-angle-spinning-induced local ordering in polymer electrolytes and its effects on solid-state diffusion and relaxation NMR measurements, *Magn. Reson. Chem.*, 2020, **58**, 1118–1129.
44 F. Kaneko, S. Wada, M. Nakayama, M. Wakihara and S. Kuroki, Dynamic Transport in Li-Conductive Polymer Electrolytes Plasticized with Poly(ethylene glycol)–Borate/Aluminate Ester, *ChemPhysChem*, 2009, **10**, 1911–1915.
45 M. Chintapalli, *et al.*, Relationship between Conductivity, Ion Diffusion, and Transference Number in Perfluoropolyether Electrolytes, *Macromolecules*, 2016, **49**, 3508–3515.
46 G. E. Murch, The haven ratio in fast ionic conductors, *Solid State Ion*, 1982, **7**, 177–198.
47 H. K. Kashyap, H. V. R. Annapureddy, F. O. Raineri and C. J. Margulis, How is charge transport different in ionic liquids and electrolyte solutions?, *J. Phys. Chem. B*, 2011, **115**, 13212–13221.
48 A. Marcolongo and N. Marzari, Ionic correlations and failure of Nernst-Einstein relation in solid-state electrolytes, *Phys. Rev. Mater.*, 2017, **1**, 025402.
49 N. M. Vargas-Barbosa and B. Roling, Dynamic Ion Correlations in Solid and Liquid Electrolytes: How Do They Affect

Charge and Mass Transport?, *ChemElectroChem*, 2020, **7**, 367–385.

50 U. H. Choi, *et al.*, Dielectric and viscoelastic responses of imidazolium-based ionomers with different counterions and side chain lengths, *Macromolecules*, 2014, **47**, 777–790.

51 J. R. Sangoro and F. Kremer, Charge transport and glassy dynamics in ionic liquids, *Acc. Chem. Res.*, 2012, **45**, 525–532.

52 Y. Wang, *et al.*, Examination of methods to determine free-ion diffusivity and number density from analysis of electrode polarization, *Phys. Rev. E: Stat., Nonlinear, Soft Matter Phys.*, 2013, **87**, 042308.

53 J. E. Kelly, J. F. Cordaro and M. Tomozawa, Correlation effects on alkali ion diffusion in binary alkali oxide glasses, *J. Non-Cryst. Solids*, 1980, **41**, 47–55.

54 J. B. Goodenough, H. Y. P. Hong and J. A. Kafalas, Fast Na^+ -ion transport in skeleton structures, *Mater. Res. Bull.*, 1976, **11**, 203–220.

55 M. Weiss, D. A. Weber, A. Senyshyn, J. Janek and W. G. Zeier, Correlating Transport and Structural Properties in $Li_{1+x}Al_xGe_{2-x}(PO_4)_3$ (LAGP) Prepared from Aqueous Solution, *ACS Appl. Mater. Interfaces*, 2018, **10**, 10935–10944.

56 K. Arbi, W. Bucheli, R. Jiménez and J. Sanz, High lithium ion conducting solid electrolytes based on NASICON $Li_{1+x}Al_xM_{2-x}(PO_4)_3$ materials (M = Ti, Ge and $0 \leq x \leq 0.5$), *J. Eur. Ceram. Soc.*, 2015, **35**, 1477–1484.

57 F. Croce, G. B. Appetecchi, L. Persi and B. Scrosati, Nanocomposite polymer electrolytes for lithium batteries, *Nature*, 1998, **394**, 456–458.

58 A. S. Best, J. Adebahr, P. Jacobsson, D. R. MacFarlane and M. Forsyth, Microscopic interactions in nanocomposite electrolytes, *Macromolecules*, 2001, **34**, 4549–4555.

59 J. F. Justin and A. Jankowiak, Ultra High Temperature Ceramics: Densification, Properties and Thermal Stability, *Aerospace Lab*, 2011, **3**, 1–11.

60 N. Chen, *et al.*, Biomimetic ant-nest ionogel electrolyte boosts the performance of dendrite-free lithium batteries, *Energy Environ. Sci.*, 2017, **10**, 1660–1667.

61 Z. Lin, X. Guo and H. Yu, Amorphous modified silyl-terminated 3D polymer electrolyte for high-performance lithium metal battery, *Nano Energy*, 2017, **41**, 646–653.